electronics

Article

A Miniaturized Bandpass Filter with Wideband and High Stopband Rejection Using LTCC Technology

Yue Ma [1,2,3,4], Qifei Du [1,2,3,4,*], Wei Zhang [5], Cheng Liu [1,3,4] and Hao Zhang [1,3,4]

[1] National Space Science Center, Beijing 100190, China; mayue21@mails.ucas.ac.cn (Y.M.); lc@nssc.ac.cn (C.L.); zhanghao@nssc.ac.cn (H.Z.)
[2] University of Chinese Academy of Sciences, Beijing 100190, China
[3] Beijing Key Laboratory of Space Environment Exploration, Beijing 100190, China
[4] Key Laboratory of Science and Technology on Environmental Space Situation Awareness, Chinese Academy of Sciences, Beijing 100190, China
[5] Shanghai Institute of Satellite Engineering, Shanghai 200240, China; wzhang509@126.com
* Correspondence: dqf@nssc.ac.cn

Abstract: This paper designs an L-band wide stopband bandpass filter by applying low-temperature cofired ceramic (LTCC) technology to the global positioning system (GPS) frequency band. Taking the Chebyshev filter as a prototype, an equivalent collector element (capacitive and inductor) structure is adopted to fully use the three-dimensional package structure of LTCC to reduce the filter size. The filter is integrated into an eight-layer LTCC dielectric, and the series–parallel connection of the collector elements in the resonance unit is utilized to produce out-of-band transmission zeros, while the input and output ports' capacitance is adjusted to control the bandwidth. Harmonic suppression is achieved by cascading two new compact stopband filters, while the size increase is insignificant due to LTCC technology. The simulation results are as follows: the center frequency is 1.575 GHz, 1 dB relative bandwidth is 6.3%, insertion loss in the passband is as slight as 1.6 dB, return loss is better than 30 dB, rejection bandwidth up to 16 GHz is more than 44 dB, and the volume of the whole filter is $6.2 \times 3.7 \times 0.78$ mm^3.

Keywords: L-band; LTCC technology; wide stopband; narrow passband; lumped elements

Citation: Ma, Y.; Du, Q.; Zhang, W.; Liu, C.; Zhang, H. A Miniaturized Bandpass Filter with Wideband and High Stopband Rejection Using LTCC Technology. *Electronics* **2024**, *13*, 166. https://doi.org/10.3390/electronics13010166

Academic Editor: Reza K. Amineh

Received: 10 November 2023
Revised: 9 December 2023
Accepted: 28 December 2023
Published: 29 December 2023

1. Introduction

Microwave filter is a crucial part of advanced wireless communication systems. Many microwave filters can be utilized to filter out the clutter harmonics. In recent years, given the system miniaturization requirements, especially passive component miniaturization requirements, low-temperature cofired ceramic (LTCC) technology as a new form of circuit implementation has been developed very quickly. Due to the high integration and high performance of LTCC technology, its three-dimensional encapsulation structure can be buried in the multilayer ceramic substrate passive components, thus reducing the size of the passive components to a large extent in the design of the system miniaturization [1]. Nowadays, various studies have been performed on microwave filter miniaturization, like the stepped-impedance resonator unit [2], the double-layer suspended stripline resonator unit [3], and the spiral resonator unit [4], which can reduce the resonator unit size to 1/4 wavelength. However, these resonant cells have a significant L-band size [5]. The LTCC three-dimensional structure has been employed to implement the lumped capacitive–inductive [6] as a stack in the Z-direction. The capacitive–inductive coupling is implemented between different layers, which can decrease the size of the microwave filters and produce transmission zeros (TZs) and cascaded bandstop filters. Thus, a filter with better attenuation performance is achieved.

This paper designs an L-band wide stopband bandpass filter using LTCC technology for the GPS frequency band. The filter comprises a narrow passband filter and two bandstop filters. The narrow filter generates transmission zeros (TZs) by introducing inductors based on a filter prototype containing an inverting converter. Compared to the existing narrowband filter prototype [7], the new filter prototype has TZs on the right side of the center frequency. The center frequency is 1.575 GHz, and the 1 dB relative bandwidth is 6.3%. The narrowband filters are cascaded with two bandstop filters to design a new bandstop filter. The resultant filter has three zeros in the high rejection band. It provides excellent blocking characteristics, achieving a wide bandwidth of 15.6 GHz, with a blocking rejection exceeding 44 dB. Compared with the recently developed wide stopband filters [8–10], this filter provides better stopband characteristics and a narrower passband. In addition, the size of this miniaturized narrowband filter is only 6.2 mm × 3.7 mm × 0.78 mm.

The remainder of this paper is structured as follows. The prototype circuit of the narrowband filter is introduced in Section 2. Section 3 presents the design of the three-dimensional structure of the filter. A novel bandstop filter structure is presented in Section 4. Finally, the simulation results after combining the narrowband filter with the novel bandstop filter are presented in Section 5. The advantages of the proposed filter are also described compared with the existing filters.

2. Filter Structure Design

This paper employs the proposed filter to fabricate the LC collector element filter using the LTCC process by fabricating the capacitors and inductors separately and embedding them in LTCC dielectric to realize the circuit [11]. Each component is manufactured using FerroA6M material from Ferro with a 5.9 dielectric constant, a loss angle tangent of 0.002, and a dielectric substrate thickness of 97 µm per layer (after cofiring) [12]. The conductor metal is gold, and the thickness of the metal line is 8 µm. The line design specifications, such as minimum line width, minimum line spacing, and through-hole diameter, are strictly compatible with those of the LTCC. Table 1 presents the particular efficiency requirements of the constructed bandpass filter.

Table 1. The filter's estimated indicators.

Feature	Value
1 dB passband range	1.52–1.62 GHz
Insertion loss	≤1.65 dB
Out-of-band rejection	6.2f0 ≥ 44 dB
Return loss	>30 dB
Dimension	0.036λ × 0.022λ

2.1. Filter Principle

As presented in Table 1's metrics, since the bandwidth requirements are narrow, an inverting converter is chosen to realize the bandpass filter design [13]. The inverting converter can convert the prototype shown in Figure 1, including both inductors and capacitors, into an equivalent form with only inductors or capacitors. Figure 2 [14] describes the inverting converter.

As shown in Figure 2a, an ideal input impedance Z_a inversion converter acts like a quarter-wavelength transmission line with a characteristic impedance of K at each frequency. That is, assuming an impedance is connected at one terminal, the impedance seen at the other terminal is as follows:

$$Z_a = \frac{K_{k,k+1}^2}{Z_b} \tag{1}$$

In the same way, in Figure 2b, an ideal conductance inverting converter acts similar to a quarter-wavelength transmission line containing a characteristic conductance of J at each frequency, such that the conductance is connected to one terminal, and the conductance seen from the other terminal is as follows:

$$Y_a = \frac{J_{k,k+1}^2}{Y_b} \quad (2)$$

Also, as shown in Figure 2, the mirror phase shift of the inverting converter is an odd multiple of plus or minus 90 degrees.

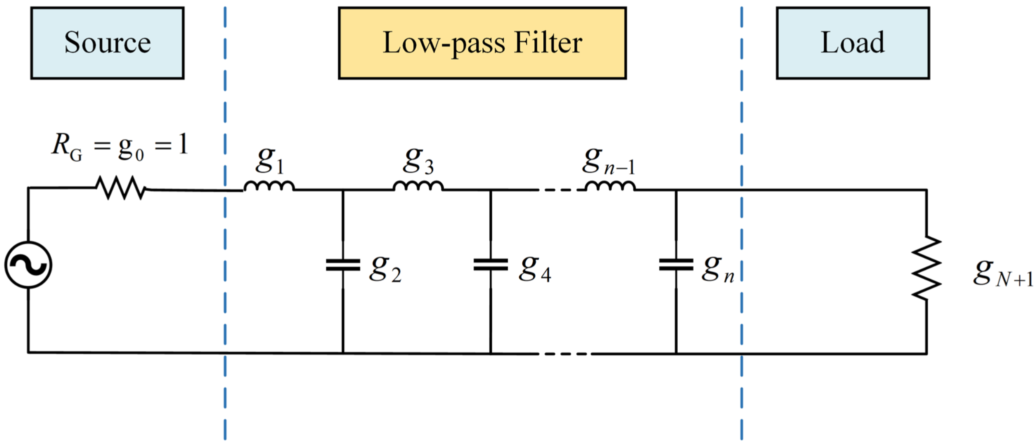

Figure 1. Low-pass filter prototype circuit.

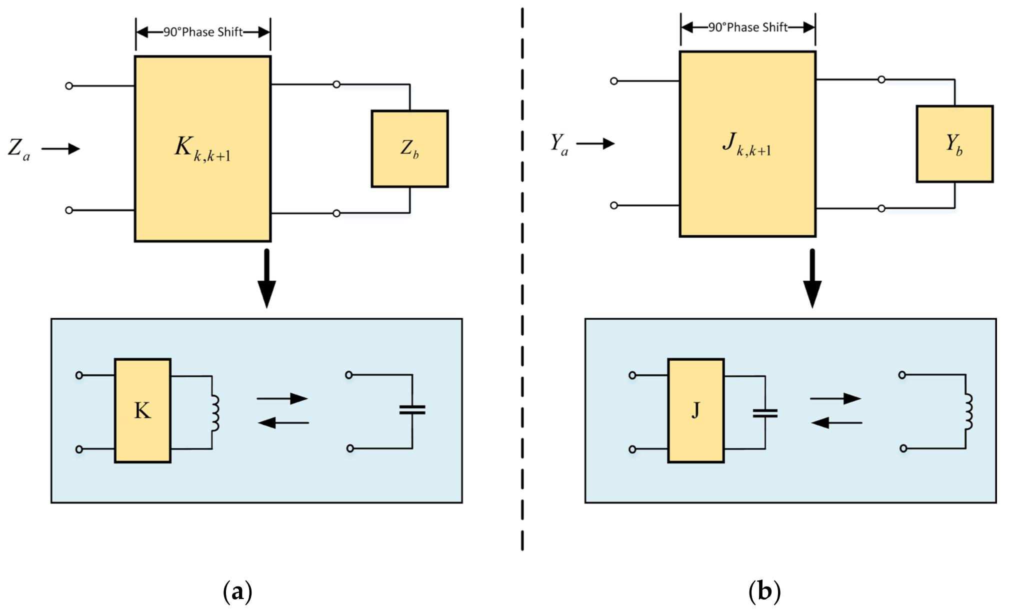

Figure 2. (**a**) Definition of an impedance inversion converter. (**b**) Definition of a conductance inversion converter.

The prototype low-pass filter circuit in Figure 1 can be transformed into two equivalent forms using the nature of the conductance inversion converter, as shown in Figure 3, including the same transmission characteristics as the low-pass prototype shown in Figure 1. Figure 3 shows a modified prototype circuit using an impedance inversion converter, where the values of G_A, G_B, and C_{rk} (C_{r1},...,C_{rn}) can be taken arbitrarily. When the parameter

$J_{k,k+1}$ of the inverting converter is obtained from Equations (3)–(5), the response will be the same as that of the filter prototype in Figure 1.

$$J_{01} = \sqrt{\frac{G_A C_{r1}}{g_0 g_1}} \tag{3}$$

$$J_{k,k+1|k=1\cdots n-1} = \sqrt{\frac{C_{rk} C_{r(k+1)}}{g_k g_{k+1}}} \tag{4}$$

$$J_{n,n+1} = \sqrt{\frac{C_{an} G_B}{g_n g_{n+1}}} \tag{5}$$

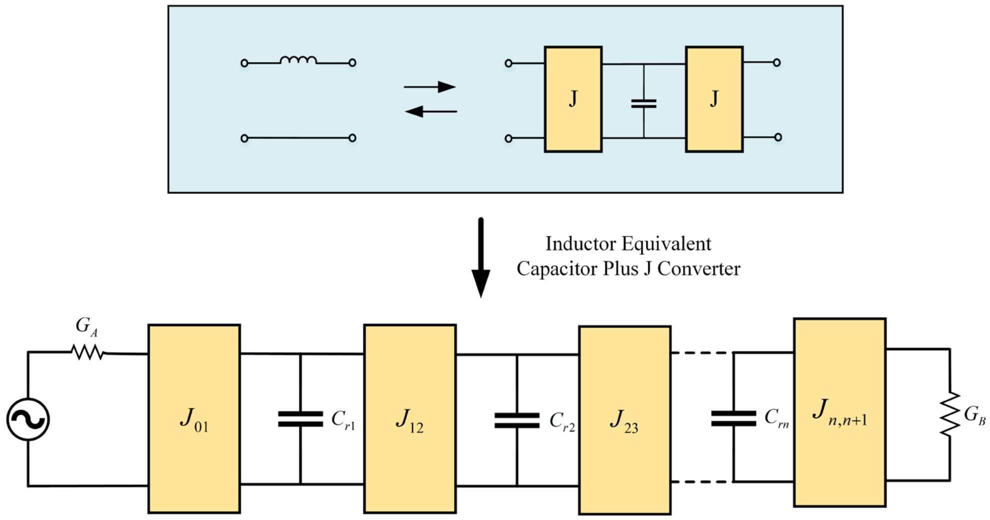

Figure 3. Modified low-pass prototype, including an impedance/conductance inverting converter.

It is essential to emphasize that g_k in the equation shown in Figure 3 (k = 0, 1, 2, ..., n + 1) is the component values of the low-pass prototype circuit described in Figure 1.

Exerting the low-pass filter to bandpass conversion on the circuit shown in Figure 3 gives a generalized bandpass filter with a conductive inverting converter and a shunt-type resonator, as shown in Figure 4.

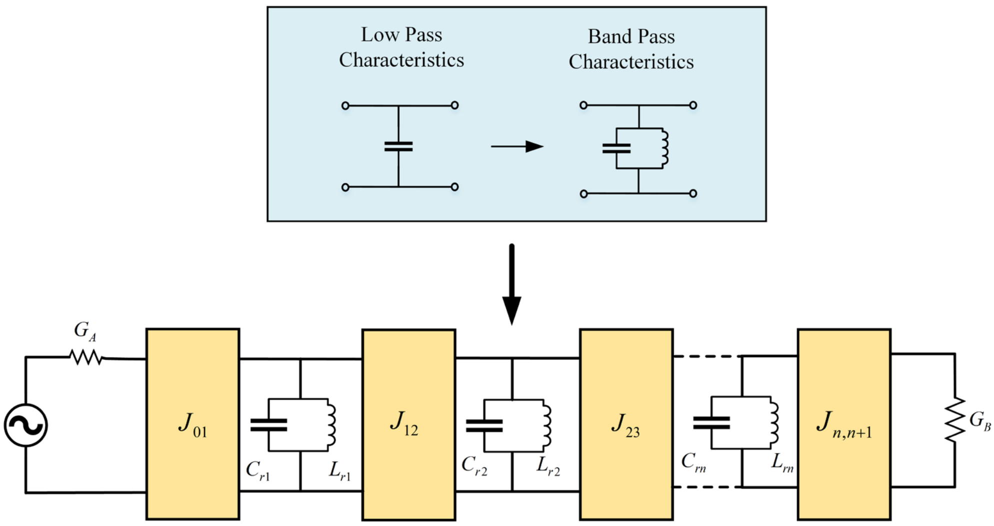

Figure 4. Coupled resonator bandpass filter transformed from Figure 3.

2.2. Filter Circuit Prototype

An inverting converter with aggregate components can be realized with different forms, such as inductive and capacitive forms, constructed with π-type and L-type structures. Among them, the capacitive form is chosen in this paper. Figure 5 shows the equivalent circuit of the above four inverting converters. It should be noted that a negative inductor (capacitor) in the circuit must be absorbed by a nearby positive inductor (capacitor), which turns out to be all positive components. Therefore, an L-structure capacitor converter is applied to both the first and last J-converters of the circuit and a π-structure capacitor converter is chosen in the middle to maintain a symmetrical structure. Taking the J inverting converter in Figure 4 as the form shown in Figure 5, a standard and specific implementation of Figure 4 can be attained using the generalized bandpass filter circuit for the conductive inverting converter mentioned in Section 2.1, as shown in Figure 6.

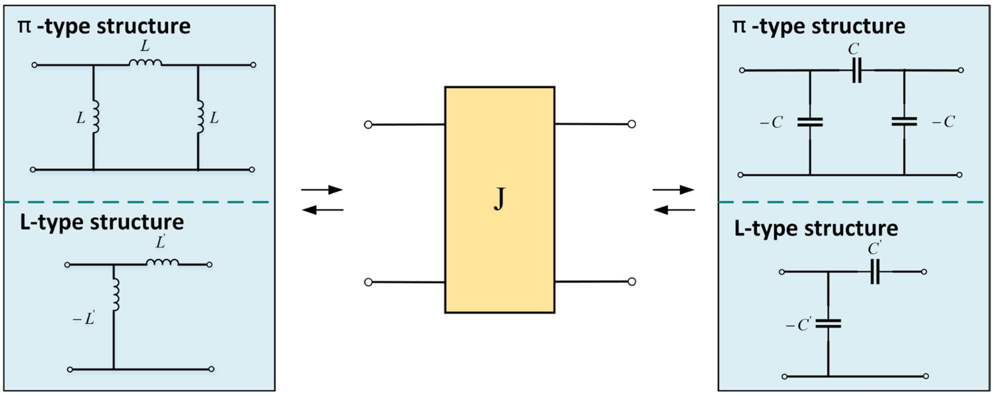

Figure 5. Specific circuit of the J inverting converter.

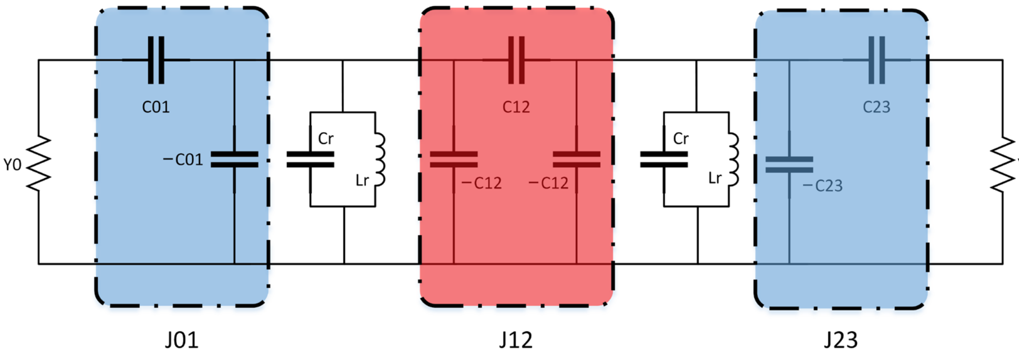

Figure 6. Transformed bandpass filter circuit.

The following formulas can determine the components of the specific circuit presented in Figure 6:

$$C_r = \frac{g}{2\pi \cdot BW \cdot Z_c} \tag{6}$$

$$L_r = \frac{2\pi \cdot BW \cdot Z_c}{g \cdot \omega_0^2} \tag{7}$$

$$b_i = \omega_0 \cdot C_{ri} \tag{8}$$

$$J_{01} = \sqrt{\frac{Y_0 \omega_0 b_1}{g_0 g_1}} \tag{9}$$

$$J_{12} = \omega_0 \sqrt{\frac{b_1 b_2}{g_1 g_2}} \tag{10}$$

$$J_{23} = \sqrt{\frac{Y_3 \omega_0 b_2}{g_2 g_3}} \tag{11}$$

$$C'_{01} = \frac{J_{0,1}}{\omega_0 \sqrt{1 - \left(\frac{J_{0,1}}{Y_0}\right)^2}} \tag{12}$$

$$C_{01} = \frac{C'_{01}}{1 + \left(\frac{\omega_0 \cdot C_{01}}{Y_0}\right)^2} \tag{13}$$

$$C'_{23} = \frac{J_{2,3}}{\omega_0 \sqrt{1 - \left(\frac{J_{2,3}}{Y_3}\right)^2}} \tag{14}$$

$$C_{23} = \frac{C'_{23}}{1 + \left(\frac{\omega_0 \cdot C_{23}}{Y_3}\right)^2} \tag{15}$$

where ω_0 is the passband center frequency, $Z_c = \frac{1}{Y_{i(i=0,3)}}$ is the characteristic impedance, g is the adjustment factor, which dictates the selection of a suitable capacitor and inductor, and BW denotes the 1 dB bandwidth. C'_{01} and C'_{23} are just intermediate values. $g_{i(i=0,1,2,3)}$ are Chebyshev values, chosen as 1, 0.843, 0.622, and 1.3554, respectively.

Based on a conductive inverted bandpass filter, an inductor L2 is added to introduce a deeper transmission zero in the filter. The Chebyshev type is modified to promote the sideband rejection. The filter's equivalent schematic is designed using the ADS software and is presented in Figure 7.

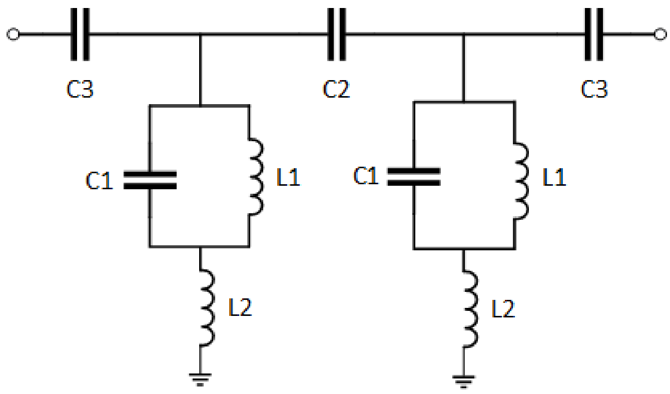

Figure 7. Narrowband filter schematic diagram.

The filter operating center frequency is 1.575 GHz, the 1 dB relative bandwidth is 100 MHz, and the initial values of the components in the equivalent circuit are obtained from Equations (6)–(12), as follows: C3 = 0.506 pF, C2 = 0.139 pF, C1 = 7.163 pF, and L1 = 1.283 nH. The value of L2 is derived directly from simulations, and the indices require wider stopband rejection. Therefore, adjusting the inductance L2 will attenuate the zero point near 6 GHz. The simulations indicate that the capacitances C2 and C3 adjust the bandwidth, C1 and L1 can adjust the passband center frequency, and L2 can adjust the TZ in Figures 8–10. As shown in Figure 8, when C2 and C3 increase, the filter bandwidth increases, and the insertion loss decreases. The filter bandwidth cannot be too narrow because it is limited by the insertion loss. Our target indicator's bandwidth and insertion loss are obtained by optimally selecting appropriate values of C2 and C3. Figure 9 shows that the center frequency of the filter passband can be adjusted very simply by adjusting the value of the inductor L1, and the same function can be achieved by adjusting the value of the capacitor C1. This paper aims to select the L1 frequency point of the GPS, thus achieving the L2 and L5 frequency points of the GPS. Figure 10 indicates that by adjusting the value of inductor L2, the high-frequency transmission zero point can be adjusted without changing the performance of the filter passband, thus attaining a good suppression effect on the high-frequency signal. This model achieves better suppression of high-frequency signals compared with the existing models, in which both of their transmission zeros are to the right of the center frequency [7]. When the two L2 inductances are equal, only one transmission zero can be generated, while the depression becomes deeper, otherwise, they will be splatted into two transmission zeros with a shallower depression depth. The former is chosen for higher suppression requirements.

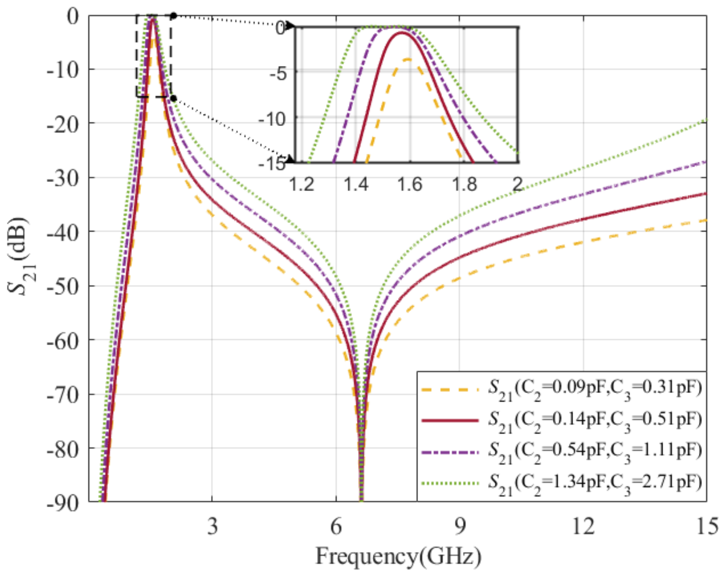

Figure 8. Effect of C2 and C3 on the filter's passband bandwidth and insertion loss.

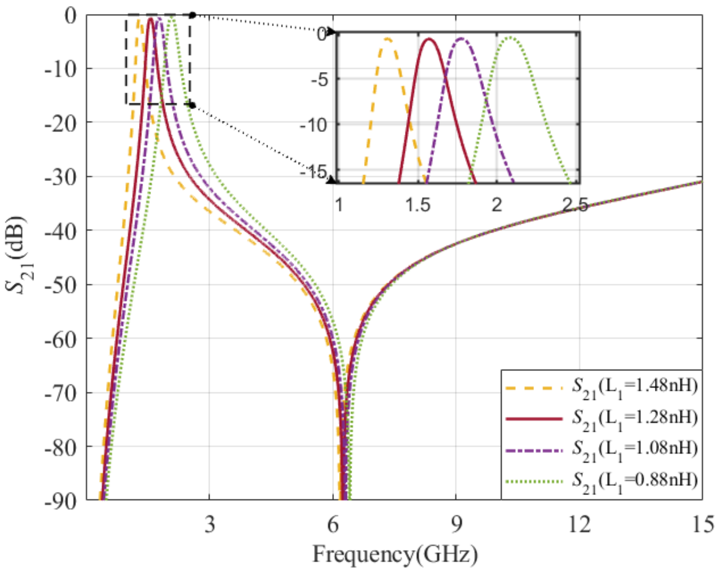

Figure 9. Effect of L1 on the filter's passband center frequency.

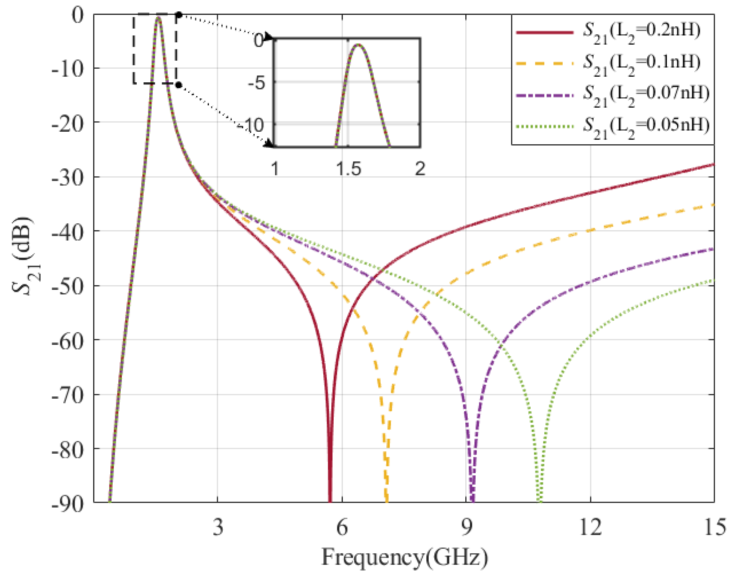

Figure 10. Effect of L2 on the filter's high-frequency transmission zeros.

3. 3D Structural Design

As the needed filter is a narrow band one, every slight adjustment to the capacitance and inductance values may influence the filter's bandwidth. Mutual coupling is necessary for the final realization of the filter using the LTCC technique. Therefore, 3D EM simulation with HFSS software is crucial in the current study [15]. The frequency model is solved using the adaptive meshing and broadband to obtain more accurate results in broadband simulations.

3.1. Capacitors

There are two main LTCC capacitors: mental insulator mental (MIM) capacitor and vertically interdigitated capacitor (VIC). VICs are the first choice for realizing capacitors with large capacitance, which can make full use of the LTCC technology's multilayer feature to increase the capacitance by increasing the number of layers. Table 2 compares the main performance and parameters of the two structures. As presented in Table 2, under the same effective capacitance value, the VIC structure has a higher self-resonant frequency (SRF), higher quality factor (Q), and a small area required for each layer while requiring many layers. The specific design makes it a reasonable choice based on the capacitance value size and the filter space layout.

Table 2. Comparison of two structures with the same effective capacitance value.

Structural Form	MIM Capacitor	VIC Capacitor
Occupied area	Large	Small
Self-resonant frequency	Slightly low	High
Q value	Slightly lower	High
Number of layers required	less	Multi

Regardless of the capacitor design framework, the relevant parameters of the capacitor element should be extracted. The capacitor is considered a two-port network, and its corresponding characteristic parameters are extracted, yielding a precise construction of the capacitor framework and dimensions. Since the capacitors in the filter have small capacitance values, i.e., C2 = 0.139 pF and C3 = 0.506 pF, the embedded MIM framework is utilized. Considering C1 = 7.163 pF, a relatively large capacitance, an embedded VIC framework is utilized to decrease the planar area.

After calculating the conductance parameter Y by HFSS, the capacitance value and quality factor parameters can be obtained as follows:

$$C_{eff} = -\frac{Im(Y(2,1))}{2\pi \cdot freq} \tag{16}$$

$$Q = -\frac{Im(Y(1,1))}{\mathrm{Re}(Y(1,1))} \tag{17}$$

where C_{eff} is the effective value of the capacitor, and freq is the self-resonant frequency.

HFSS simulation determines the physical dimensions of C1, C2, and C3. The 3D structure of C1 is presented in Figure 11a, which has orange and green colours to distinguish the two polarities of the capacitor and the capacitance simulation results are presented in Figure 11b.

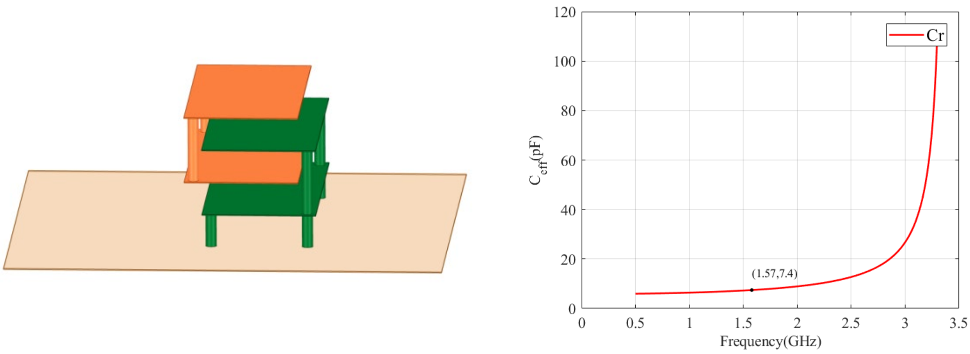

(**a**) (**b**)

Figure 11. 3D structure diagram (**a**) and simulation results of capacitor C1 (**b**).

3.2. Inductors

LTCC inductors generally include planar and spiral types. Since the Q value of the inductor is much lower than the capacitance, the inductor design plays an essential role in the filter insertion loss.

Table 3 compares the main performance and parameters of the four inductor structures. It can be seen that with the same effective inductance value, the spiral inductor has the advantages of a relatively higher resonant frequency and quality factor, a smaller single-layer area, and the disadvantage of the number of required layers, followed by the stacked, displacement, and planar structures. The specific design should choose the inductor implementation form according to the key parameters. The inductor effective value (Leff) determines the size of the total inductance, and the Q value determines the size of the inductor loss. The design of LTCC inductors should focus on the effective value of the inductance, quality factor, and self-resonant frequency SRF; the effective value of the inductance determines the size of the inductor and the specific application of the resonance frequency, the quality factor determines the loss of RF devices and other performance parameters, and the self-resonant frequency SRF determines the effective use of the inductor frequency range.

Table 3. Comparison of inductance performance of various structures with the same inductance value.

Type	Structural Form	Occupied Area	Self-Resonant Frequency	Q Value	Number of Floors
Monolayer	Planar	Maximum	Lowest	Lowest	least
	Displacement	Small	High	High	Medium
Multilayer	Stacked	Medium	Medium	Medium	Medium
	Spiral	Smallest	Highest	Highest	Most

The inductance values of L1 and L2 in the filter model are small and can be realized by a single layer of short wires or through holes to avoid the complexity caused by mutual coupling with other capacitors. The inductor's width is 0.2 mm, i.e., the 50 Ω stripline's width. HFSS simulation is employed to determine the inductor's length. Inductor L1 is the main inductor in the filter and directly affects the center frequency. A planar-type inductor is utilized to prevent mutual coupling with the other capacitors.

The LTCC's effective inductance can be described in terms of admittance parameters as follows [16]:

$$L_{eff} = \frac{Im\left(\frac{1}{Y(1,1)}\right)}{2\pi \cdot freq} \tag{18}$$

$$Q = -\frac{Im(Y(1,1))}{Re(Y(1,1))} \tag{19}$$

where freq denotes the self-resonant frequency, and Y11 is the inductor's conductance value, calculated by HFSS. Figure 12 presents the inductor's 3D model, with L1 = 1.82 nH. The conductor's width in the inductor is 0.2 mm, while the total length is 2.6 mm. Figure 12 presents the effective inductance attained through HFSS simulation.

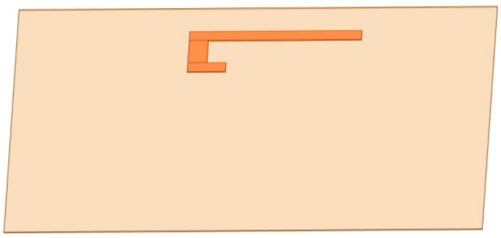

(**a**)

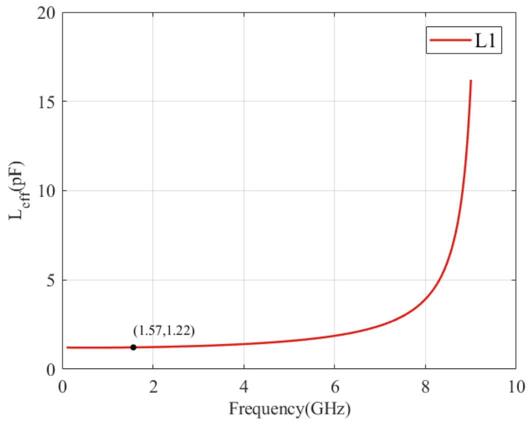

(**b**)

Figure 12. 3D structure diagram (**a**) and simulation results of inductor L1 (**b**).

3.3. Simulation Results

Based on the inductor and capacitor models, all of the filter components are modeled, simulated, and optimized in 3D. The three-dimensional structure simulation is as close as possible to the actual situation; a FerroA6M material is selected as the substrate material, the metal line material is set to gold, and the thickness is 8 μm. As shown in Figure 7, there are four inductors and five capacitors with different capacitance values. These nine variables pose a great difficulty in the modeling and optimization process. In order to facilitate modeling and optimization, the current study employs a symmetric circuit framework. Nine variables are reduced to five using the model's symmetry, thus simplifying the LTCC. Figure 13 presents the LTCC bandpass filter's 3D model. It is worth mentioning that to show the picture more clearly, the model layer spacing is enlarged five times, and the other dimensions and the layer spacing are kept unchanged. The 3D model parameters are as follows:

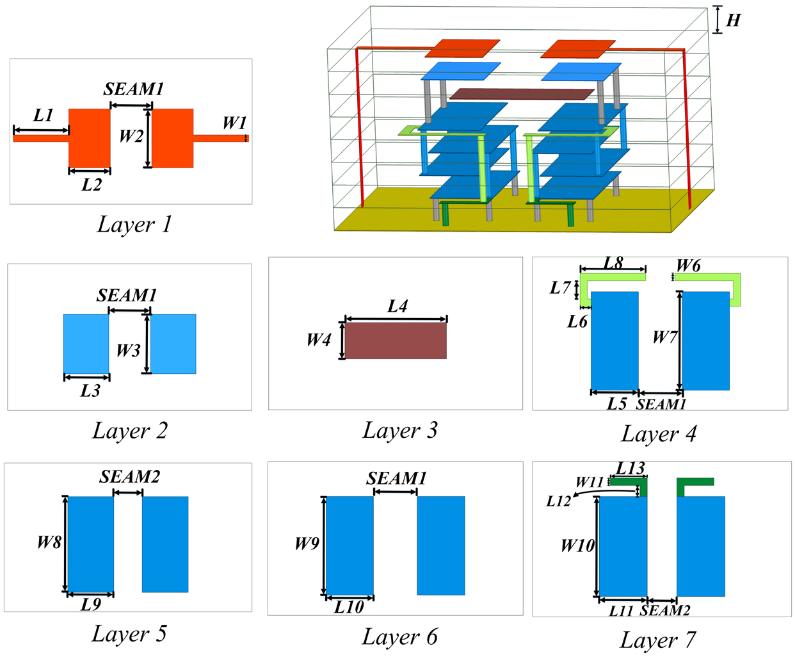

Figure 13. 3D modeling of LTCC bandpass filters.

SEAM = L2 = 1.2 mm, L1 = 1.5 mm, W1 = W6 = W11 = 0.2 mm, W2 = W3 = 1.7 mm, L4 = 3.6 mm, W4 = L13 = 1 mm, L6 = L12 = 0.3 mm, L7 = 0.5 mm, L8 = 1.8 mm, W7 = W8 = W9 = W10 = 2.7 mm, L3 = L5 = L9 = L10 = L11 = 1.3 mm, and H = 97 µm.

By verifying the simulation outcomes of the flexible layout of inductors and capacitors in the model, the model is continuously optimized and adjusted to obtain the optimum simulation results, as presented in Figure 14. The simulation results indicate that in the 1.525–1.625 bandwidth, the insertion loss is relatively slight, the return loss meets the requirements, and the TZ is near 6 GHz. However, since there is a resonance near 9.5 GHz, a new bandstop filter should be introduced to eliminate the resonance.

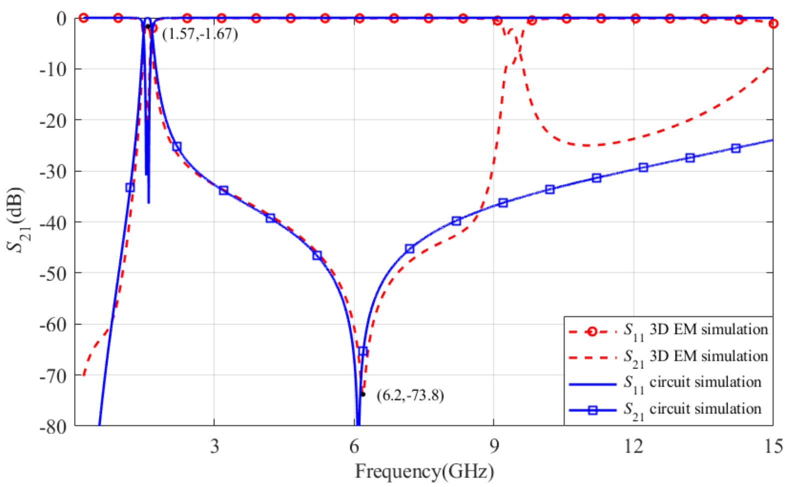

Figure 14. LTCC bandpass filter simulation results.

4. Wide Stopband Filter Design

4.1. Principle of the Wide Stopband Filter

The metrics in Table 1 indicate the relatively high out-of-band rejection requirement of the filter. There are two methods to improve the filter's out-of-band rejection when designing the filter: increasing the filter's order and adding the TZs. However, as the order increases, the filter size increases [17], which is inappropriate for designing miniaturized filters. Therefore, transmission zeros are generally added when constructing the miniaturized filters [18,19]. The filter's zero frequency is the frequency that makes the transmission equation zero. Ideally, since energy cannot pass through the zero frequency, excellent isolation can be attained. The set parameter mode generally adopts series or parallel resonances.

When the capacitance and inductance in a circuit are connected in series or parallel, the impedance and conductance in a high-frequency circuit are calculated as follows:

$$jX(\omega) = j\omega C + \frac{1}{j\omega L} \tag{20}$$

$$jB(\omega) = j\omega L + \frac{1}{j\omega C} \tag{21}$$

According to Equation (20), an open circuit is obtained as the conductance in a parallel resonant circuit is zero, entirely reflecting the energy at that frequency, thus constructing a transmission zero. According to Equation (21), when the LC satisfies the resonance relation, the input impedance in the series resonant circuit becomes zero, causing a short circuit. The whole energy at the mentioned frequency is absorbed, forming a TZ.

4.2. Three-Dimensional Structural Design

This bandstop filter adopts the form of Figure 15b; the inductor is realized using a narrow wire inductor with an over-hole, and the capacitor is only realized using a flat-plate capacitor. Figure 16 shows the three-dimensional structural model diagram.

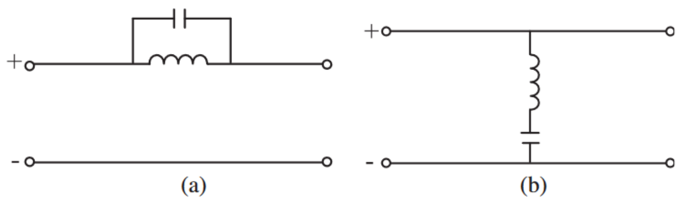

Figure 15. (**a**) Parallel resonant circuit. (**b**) Series resonant circuit.

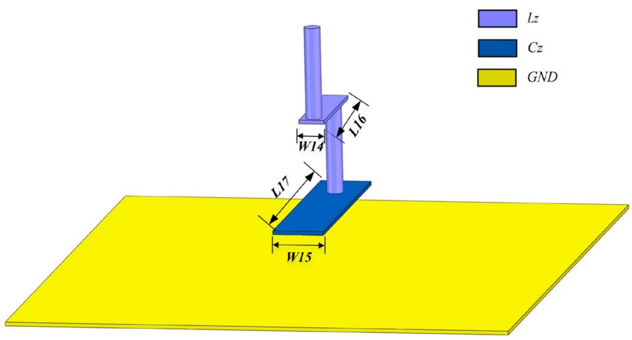

Figure 16. 3D model diagram of the band reject filter.

4.3. Simulation Results

The band reject filter can change the resonance point by adjusting the inductor length Lz or the flat size of the capacitor Cz, as shown in Figure 16, by changing the capacitor width W15 and thus changing the resonance frequency point. As W15 increases, the capacitance Cz increases, and the resonance point is shifted to a lower frequency, compatible with the theoretical analysis. Figure 17 shows the simulation results. This simulation is only performed for the bandstop filter. The following section presents the adjustment of the transmission zeros of the target filter after cascading the narrowband filter with the bandstop filter.

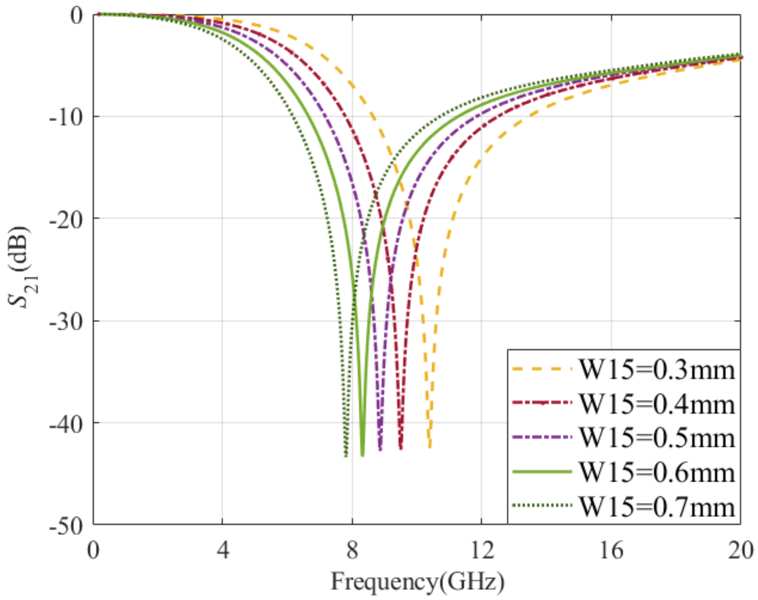

Figure 17. Simulation results of the band reject filter.

5. Overall Simulation

5.1. Simulation Results

The model diagram after cascading the bandpass filter designed in Section 3 with two new bandstop filters, as shown in Figure 18, is designed to achieve the wide stopband index requirement. Figure 18 shows the equivalent circuit diagrams of the corresponding lumped elements. Figure 19 marks different lumped elements with different colors, each corresponding to that in Figure 18, and the overall structure shows symmetry. The model parameters are W12 = W14 = 0.2 mm, L14 = L16 = 1 mm, L15 = 2 mm, W13 = W15 = 0.5 mm, and L17 = 1.6 mm. Figure 20 shows the exterior view of the filter when placed on an RO4350B substrate. RO4350B can be well applied to high-frequency circuits. The substrate thickness is h = 0.508, and the dielectric constant is ε = 3.66. The transmission line to the filter inputs and outputs is of the CPW ground-type, matched to 50 ohms to match the filter inputs and outputs. For better matching, tapered transmission lines are added close to the input and output of the filter. The line width is 0.48 mm, and the line gap is 0.24 mm. As shown in Figure 21, the transmission zeros of the target filter are adjusted by adjusting the size of the capacitor Cz. The results indicate that as L15 decreases, the transmission zeros move to higher frequencies. When the frequency of transmission zero 3 (TZ3) is too high, the transmission zeros should be placed appropriately to successfully suppress the harmonics. The second transmission zero 2 (TZ2) is adjusted similarly to TZ3 by controlling TZ2 and adjusting the size of the capacitance on the other side. Figure 10 illustrates the control of the first transmission zero 1 (TZ1). The filter with the best stopband characteristics is obtained by adjusting the three transmission zeros. Figure 22 shows the HFSS simulation of this bandpass filter. As shown in Figure 22, compared with ADS simulation, these two simulations have relatively close transmission results, indirectly demonstrating the feasibility of the equivalent circuit.

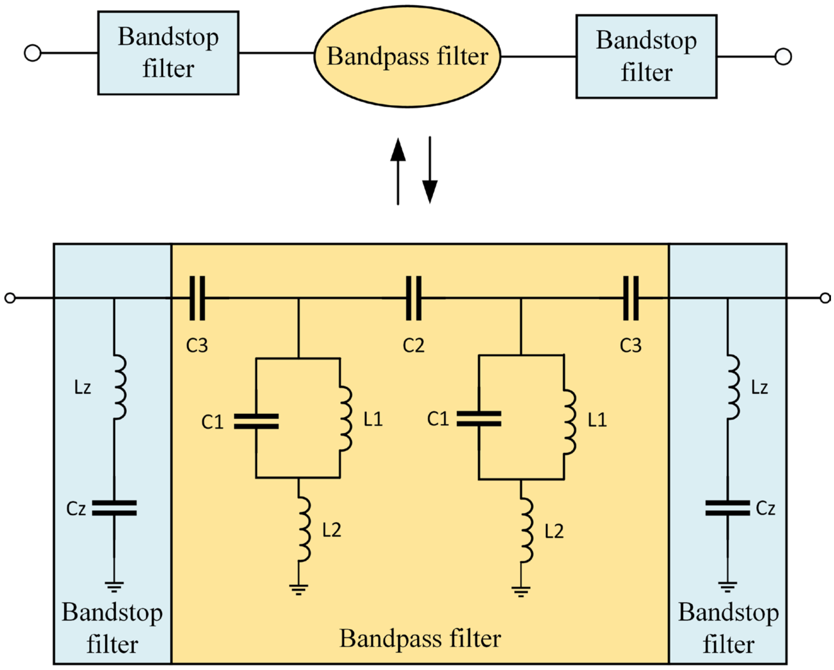

Figure 18. Wide stopband narrow bandpass filter schematic diagram.

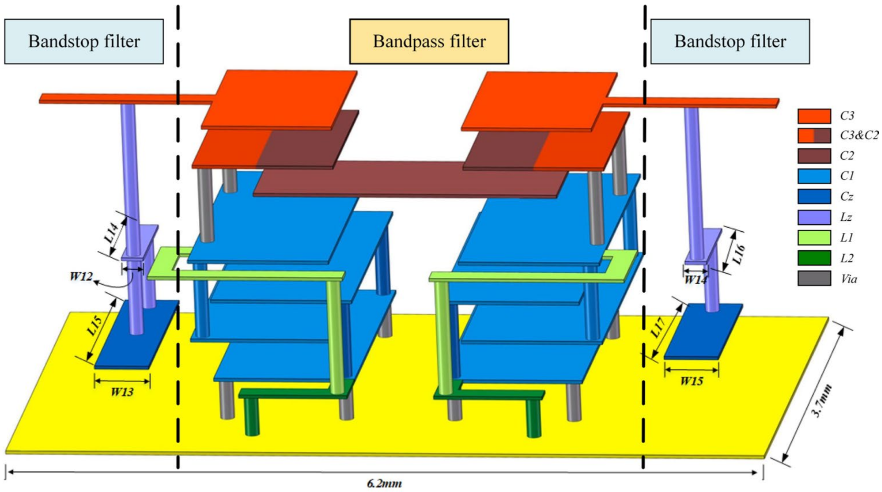

Figure 19. Three-dimensional structure of a wide stopband narrow bandpass filter.

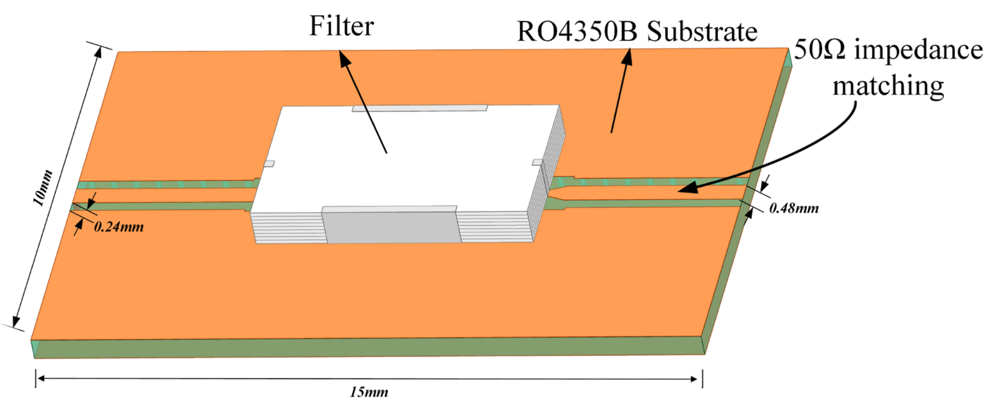

Figure 20. Exterior view of the wide stopband narrow bandpass filter.

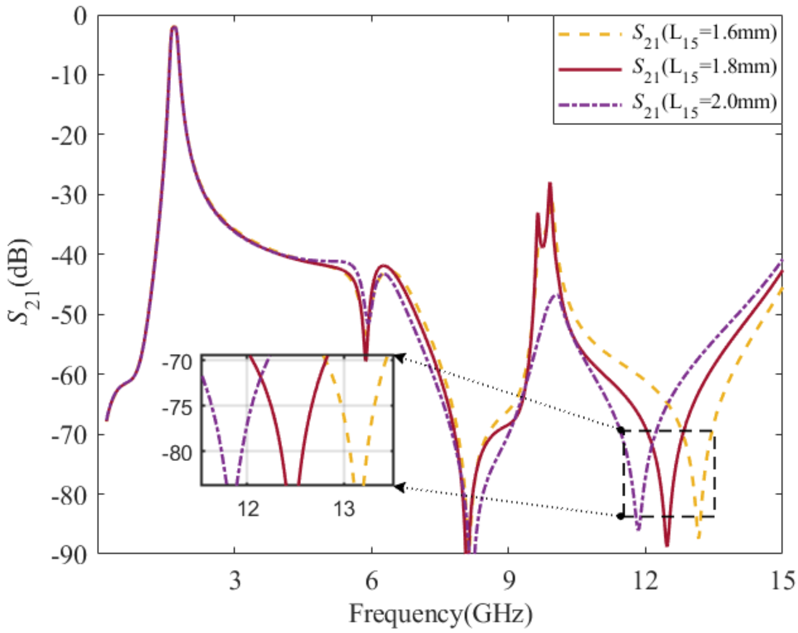

Figure 21. Effect of L15 on the filter's high-frequency transmission zero 3.

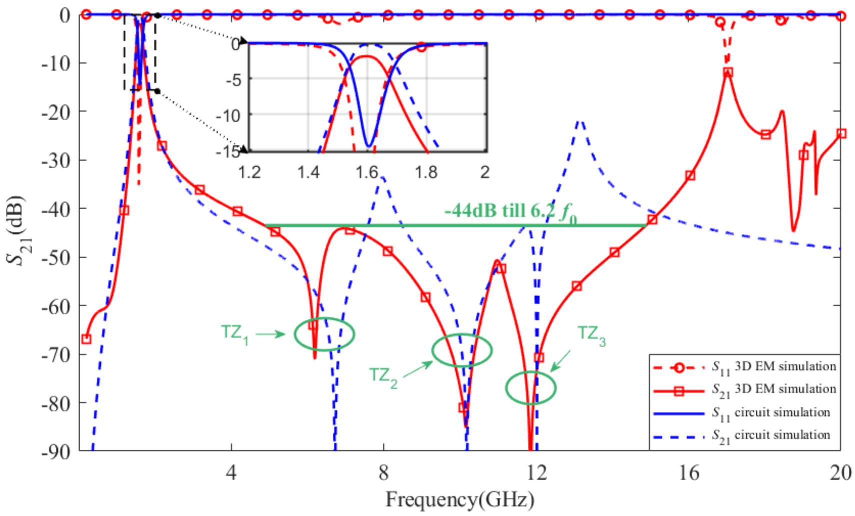

Figure 22. Simulation results of the wide stopband narrow bandpass filter.

5.2. Performance Comparison

Table 4 compares the efficiency of the constructed L-band bandpass filter with previously published studies.

Table 4. Comparison with previous studies.

Refs.	F0 (GHz)	FBW (%)	IL (dB)	Stopband Bandwidth	Rejection Level (dB)	Core Size (λ_g^2)	Selectivity Factor (%)
[20]	0.835	15.8%	0.41	4.26f_0	<20 dB	0.16 ∗ 0.12	32.51@20 dB
[21]	5.5	18.2%	2.46	1.02f_0	<32 dB	0.058 ∗ 0.029	9.9@32 dB
[22]	0.75	12.8%	0.6	5.2f_0	<20 dB	0.014 ∗ 0.02	5.87@20 dB
[23]	6.11	8.96	1.07	2.05f_0	<22 dB	0.153 ∗ 0.194	32.22@20 dB
[24]	3.5	22.9%	0.5	1.64f_0	<18 dB	0.09 ∗ 0.09	13.0@20 dB
This work	1.57	6.3%	1.65	6.2f_0	<44 dB	0.036 ∗ 0.022	110@20 dB 75.98@40 dB

Table 4 shows that compared with the studies performed in the last five years (the studies [20,21,23,24]), the proposed filter occupies less space by stacking the collector elements in the Z-direction through the LTCC process. Compared with the literature [20–24], focusing on wide stopband bandpass filters, the designed filter provides better stopband characteristics and narrower bandwidth, with moderate insertion loss. As shown in Table 4, the proposed filter has an excellent selectivity factor (SF), which is crucial for wide stopband filters.

6. Conclusions

The current study describes a bandpass filter with narrowband and considerable out-of-band rejection for the GPS band. The filter framework can be simplified and the simulation complexity can be alleviated using symmetry. By the new filter prototype and cascading the new three-dimensional structure of the bandstop filter, three TZs are produced to promote the filter's stopband characteristics significantly. LTCC technology has a significant advantage in realizing the filter's miniaturization, leading to a size of 6.2 mm $*$ 3.7 mm $*$ 0.78 mm, smaller than the conventional process filter. The whole circuit has the advantages of high performance, small size, and low cost (in the case of mass production), making it suitable for GPS wireless communication-integrated systems and GPS L1 frequency pre-filtering applications.

In the future development of integration technology, the requirements for the performance and miniaturization of communication systems will also increase. Thus, creating miniaturized filters with LTCC technology will be one of the future development trends. In addition, with the development of wireless technology, the spectrum's utilization is becoming increasingly important. Therefore, filtering signals at other frequencies will also become more and more critical.

Author Contributions: Conceptualization, Y.M., Q.D., W.Z. and C.L.; methodology, Y.M. and Q.D.; software, Y.M.; validation, Y.M., W.Z., C.L. and H.Z.; investigation, Y.M., Q.D. and C.L.; writing—original draft preparation, Y.M. and Q.D.; writing—review and editing, Y.M., Q.D., W.Z., C.L. and H.Z. All authors have read and agreed to the published version of the manuscript.

Funding: This research received no external funding.

Data Availability Statement: https://www.scidb.cn/en/s/2MFZFb (accessed on 8 November 2023).

Acknowledgments: Qifei Du and Cheng Liu are gratefully acknowledged for their insightful comments and helpful discussions.

Conflicts of Interest: The authors declare no conflicts of interest.

References

1. Ihle, M.; Ziesche, S.; Zech, C.; Baumann, B. Compact LTCC packaging and printing technologies for Sub–THz modules. In Proceedings of the 2018 7th Electronic System-Integration Technology Conference (ESTC), Dresden, Germany, 18–21 September 2018.
2. Tang, J.M.; Liu, H.W.; Yang, Y. Balanced dual-band superconducting filter using stepped-impedance resonators with high band-to-band isolation and wide stopband. *IEEE Trans. Circuits Syst. II Express Briefs* **2021**, *68*, 131–135. [CrossRef]
3. Xia, L.; Wu, B.; Song, L.; Chen, J.Z.; Cheng, Q.S. Design of pseudoelliptic filters with controllable transmission zeros using high-Q double-layer suspended stripline resonators. *Int. J. RF Microw. Comput. Aided Eng.* **2019**, *29*, e21785. [CrossRef]
4. Xu, K.D.; Xu, H.; Liu, Y.H.; Ai, J.; Liu, Q.H. Short- and open-stub loaded spiral resonator and its application in planar microstrip filters. *IET Microw. Antennas Propag.* **2017**, *11*, 363–369. [CrossRef]
5. Kim, C.H.; Chang, K. Wide-stopband bandpass filters using asymmetric stepped-impedance resonators. *IEEE Microw. Wirel. Compon. Lett.* **2013**, *23*, 69–71. [CrossRef]
6. Arabi, E.; Lahti, M.; Vähä-Heikkilä, T.; Shamim, A. A 3-D miniaturized high selectivity bandpass filter in LTCC technology. *IEEE Microw. Wirel. Compon. Lett.* **2014**, *24*, 8–10. [CrossRef]
7. Tan, C.; Yu, Z.J.; Xie, C.S. An L-band bandpass filter with narrow bandwidth and miniature based on LTCC technology. *Prog. Electromagn. Res.* **2019**, *87*, 63–72. [CrossRef]
8. Peng, Z.; Zhou, J.; Rao, Y.B.; Deng, Z.X.; Luo, X. Compact bandpass filter with wide stopband and low radiation using fully-packaged substrate integrated defected ground structure. In Proceedings of the 2021 IEEE International Symposium on Radio-Frequency Integration Technology (RFIT), Hualien, Taiwan, 25–27 August 2021.

9. Li, S.X.; Ma, K.X.; Chen, X.; Yan, N.N.; Fu, H.P. A miniaturized bandpass filter with wideband and high stopband rejection using LTCC technology. In Proceedings of the 2020 IEEE Asia-Pacific Microwave Conference (APMC), Hong Kong, China, 8–11 December 2020.
10. Feng, W.J.; Gao, X.; Che, W.Q.; Yang, W.C.; Xue, Q. LTCC wideband bandpass filters with high performance using coupled lines with open/shorted stubs. *IEEE Trans. Compon. Packaging Manuf. Technol.* **2017**, *7*, 602–609. [CrossRef]
11. Dai, Y.S.; Xu, L.; Han, Q.F.; Chen, S.B.; Wang, L.J.; Chen, R.Q. Miniaturized LTCC wideband bandpass filter using lumped-element shunt LC resonators. In Proceedings of the 2012 International Conference on Microwave and Millimeter Wave Technology (ICMMT), Shenzhen, China, 5–8 May 2012.
12. Du, J.C.; Chen, N.; Lu, Q.Y. Design of a Ka-band Microstrip quasi-Yagi antenna array based on LTCC substrate. In Proceedings of the 2013 IEEE International Conference on Microwave Technology & Computational Electromagnetics, Qingdao, China, 25–28 August 2013.
13. Matthaei, G.L.; Young, L.; Jones, E.M.T. *Microwave Filters, Impedance-Matching Networks, and Coupling Structures*; Artech House, Inc.: Boston, MA, USA, 1980.
14. Hong, J.S.; Lancaster, M.J. Advanced RF/microwave filters. In *Microstrip Filters for RF/Microwave Applications*; Hong, J.S., Lancaster, M.J., Eds.; John Wiley & Sons, Ltd.: New York, NY, USA, 2001; pp. 315–377.
15. Leung, W.Y.; Cheng, K.K.M.; Wu, K.L. Multilayer LTCC bandpass filter design with enhanced stopband characteristics. *IEEE Microw. Wirel. Compon. Lett.* **2002**, *12*, 240–242. [CrossRef]
16. Wu, J.J.; Yan, B.; Zhang, Q.S.; Guo, G.F.; Su, H. Design and parameters extraction methods of microwave LTCC embedded inductor. *Telecommun. Eng.* **2007**, 123–126. (In Chinese)
17. Zhu, L.F. Narrowband LTCC filter with length-reduced end-coupled resonators. *Prog. Electromagn. Res. Lett.* **2020**, *93*, 13–19. [CrossRef]
18. Dai, Y.S.; Zhang, H.S.; Qi, G.P.; Lu, D.L.; Tao, Z.L.; Qian, G.X.; Wang, H. LTCC bandpass filter for Bluetooth™ application with dual transmission zeros. In Proceedings of the 2008 International Conference on Microwave and Millimeter Wave Technology, Nanjing, China, 21–24 April 2008.
19. Cui, L.W.; Yu, J.G.; Li, S.L.; Liu, Y.N. A sharp-rejection dual-bandstop filter with multiple transmission poles and zeros based on transversal signal-interaction concepts. In Proceedings of the 2017 IEEE 5th International Symposium on Electromagnetic Compatibility (EMC-Beijing), Beijing, China, 28–31 October 2017.
20. Barik, R.K.; Koziel, S.; Pietrenko-Dabrowska, A. Broad stopband, low-loss, and ultra-compact dual-mode bandpass filter based on HMSIRC. *Electronics* **2023**, *12*, 2831. [CrossRef]
21. Li, Y.L.; Zhu, X.; Liu, J.C.; Zhou, L.J.; Wang, Z.H. Miniaturization of low temperature co-fired ceramic packaging for microwave filters. In Proceedings of the 2018 19th International Conference on Electronic Packaging Technology (ICEPT), Shanghai, China, 8–11 August 2018.
22. Chen, L.; Yang, Z.H.; Ling, S.X.; Ding, D.W. Design of LTCC bandpass filter with broadband external suppression for 5G applications. In Proceedings of the 2023 International Conference on Microwave and Millimeter Wave Technology (ICMMT), Qingdao, China, 14–17 May 2023.
23. Duraisamy, T.; Barik, R.K.; Cheng, Q.S.; Kamakshy, S.; Sholampettai Subramanian, K. Miniaturized SIW filter using D-shaped resonators with wide out-of-band rejection for 5G applications. *J. Electromagn. Waves Appl.* **2020**, *34*, 2397–2409. [CrossRef]
24. Tie, H.Y.; Luo, L.; Song, Z.C.; Ma, Q.; Hu, S.W.; Zhou, B. Dual-mode LTCC filter with 4th-order harmonic suppression for 5G N78 applications. In Proceedings of the 2021 International Conference on Microwave and Millimeter Wave Technology (ICMMT), Nanjing, China, 23–26 May 2021.